The Pervasive Presence of Fluctuating Oxygenation in Tumors

Laura I. Cárdenas-Navia,[1] Daniel Mace,[2] Rachel A. Richardson,[3] David F. Wilson,[4] Siqing Shan,[3] and Mark W. Dewhirst[3]

[1]Department of Biomedical Engineering and [2]Computational Biology and Bioinformatics Program, Duke University; [3]Department of Radiation Oncology, Duke University Medical Center, Durham, North Carolina; and [4]Department of Biochemistry and Biophysics, University of Pennsylvania Medical Center, Philadelphia, Pennsylvania

Abstract

Tumor hypoxia is a persistent obstacle for traditional therapies in solid tumors. Strategies for mitigating the effects of hypoxic tumor cells have been developed under the assumption that chronically hypoxic tumor cells were the central cause of treatment resistance. In this study, we show that instabilities in tumor oxygenation are a prevalent characteristic of three tumor lines and previous characterization of tumor hypoxia as being primarily diffusion-limited does not accurately portray the tumor microenvironment. Phosphorescence lifetime imaging was used to measure fluctuations in vascular pO_2 in rat fibrosarcomas, 9L gliomas, and R3230 mammary adenocarcinomas grown in dorsal skin-fold window chambers (n = 6 for each tumor type) and imaged every 2.5 minutes for a duration of 60 to 90 minutes. O_2 delivery to tumors is constantly changing in all tumors, resulting in continuous reoxygenation events throughout the tumor. Vascular pO_2 maps show significant spatial heterogeneity at each time point, as well as between time points. The fluctuations in oxygenation occur with a common periodicity within and between tumors, suggesting a common mechanism, but have tumor type–dependent spatial patterns. The widespread presence of fluctuations in tumor oxygenation has broad ranging implications for tumor progression, stress response, and signal transduction, which are altered by oxygenation/reoxygenation events. [Cancer Res 2008;68(14):5812–9]

Introduction

Tumor hypoxia is one of the most studied physiologic phenomena in cancer research and has been shown to be prognostically significant in many clinical studies, independent of treatment type (1–3). Since the discovery of diffusion limited tumor hypoxia in the 1960s, most strategies for overcoming or targeting hypoxic areas in tumors have been developed using a paradigm of chronically hypoxic areas in tumors or areas of hypoxia that are oxygen-deficient because they are beyond the typical diffusion limit of O_2. Although many investigators have measured the presence of so-called intermittent or acute hypoxia in preclinical (4–11) and clinical tumors (12), instabilities in tumor oxygenation were presumed to be temporally rare, spatially isolated events attributed to transient episodes of vascular stasis (6, 7, 13–16).

Our group previously showed that vascular stasis was not necessary for tissue to experience transient hypoxia; alternatively, fluctuations in red cell flux could easily cause this effect (17). Based on a series of studies, we have advocated the concept that instabilities in red cell flux are the norm within tumors and that this condition could lead to widespread instability in oxygenation throughout a tumor. Because oxidative stress has been shown to cause a differential cellular response for intermittent versus chronic hypoxia in tumor and endothelial cells (18–25), the pervasive presence of fluctuating oxygenation in tumors has consequential implications for our understanding of tumor progression, stress response, and signal transduction; in all studies, intermittent hypoxia has been shown to increase molecular or physiologic responses in a manner consistent with more malignant tumor phenotypes (18–25).

In this study, we show data directly measuring temporal fluctuations in vascular pO_2 in three rat tumors, characterizing the spatial and temporal differences. We show that O_2 delivery to tumors is constantly fluctuating, resulting in reoxygenation events throughout the tumor.

Materials and Methods

Dorsal skin flap window chamber. Tumors were grown in the dorsal skin flap window chambers in female Fischer 344 rats (150–175 g). The rats were surgically implanted with titanium window chambers as previously described (26). A small piece of tumor ~1 mm^3 from a donor animal was transplanted onto the fascia at the time of surgery, and glass windows were placed on both sides of the chamber. Three rat tumor lines were studied: R3230Ac mammary adenocarcinoma (n = 6), FSA fibrosarcoma (n = 6; ref. 27), and 9L glioma (n = 6; ref. 28).

At 2 to 4 d after surgery, animals were shipped from Duke University Medical Center to University of Pennsylvania and allowed to acclimate for 4 to 7 days before any measurements were taken. All experimental protocols were approved by Duke University Medical Center and University of Pennsylvania Institutional Animal Care and Use Committees.

Phosphorescence lifetime imaging. Phosphorescence lifetime imaging (PLI) was performed on the tumors in the dorsal window chamber using a previously described imaging set-up (29).

Experimental protocol. Tumors were selected for imaging as they reached a diameter of ~3 mm. Rats were anesthetized with 50 mg/kg pentobarbital i.p. for imaging; this dose is known to maintain stable heart rate and blood pressure within a range reported for unanesthetized rats (30) over a period of several hours (11) and we have previously shown that blood oxygen content is equivalent to unanesthetized rats using this method (31). Before taking any measurements, the femoral vein was cannulated and the rat was placed in lateral recumbancy on a temperature-controlled heating pad onto the stage with the tumor side of the window chamber facing the camera. The window chamber was secured using a custom-made holder attached directly to the stage so that the glass window laid flat. Once secured and immobile, neither the rat nor the microscope stage were touched to maintain the same location for sequential images on the camera.

0.3 mL of 8 mg/kg phosphor G_2 (32) was then injected i.v. into the animal, and imaging began. The field of view for the image was chosen randomly within the tumor, although care was taken to ensure that the entire field of view was tumor tissue and not normal tissue. Images were

Note: Supplementary data for this article are available at Cancer Research Online (http://cancerres.aacrjournals.org/).

Requests for reprints: Mark W. Dewhirst, Box 3455, Room 201 MSRB, Research Drive, Duke University Medical Center, Durham, NC 27710. Phone: 919-684-4180; Fax: 919-684-8718; E-mail: dewhirst@radonc.duke.edu.

doi:10.1158/0008-5472.CAN-07-6387

taken every 2.5 min for 60 to 90 min before the animal was sacrificed with an overdose of pentobarbital i.v., and a final image was taken. Experiments in which the pO_2 did not drop to near zero after the animal was sacrificed were discarded ($n = 2$; these experiments are not included in the $n = 6$ for each tumor type).

Phosphor G_2 was excited using light at 450 nm, which penetrates ~ 50 μm into the tumor tissue (32); therefore, PLI images reflect the oxygenation status of vessels near the surface of the tumor.

Image analysis. Each PLI image yielded a 2.2 × 2.85 mm (480 × 752 pixels) map of vascular pO_2 at each time point. The maps of vascular pO_2 were imported into MATLAB, and all further analyses were done in MATLAB. Pixels from the original maps were averaged over every 4 × 4 pixels and a new, averaged map of vascular pO_2 was created (120 × 188 pixels; each pixel is 15.2 × 18.3 μm). This averaged map of vascular pO_2 was used for all subsequent analyses. Analyses are presented in terms of pixel sizes; the light signal from the tissue scatters laterally before it is captured by the PLI camera, which is several centimeters away from the surface of the window. Therefore, the signal from any given pixel contains a contribution from the surrounding pixels.

In an initial exploratory analysis, sequential time images were subtracted, i.e., time point 1 subtracted from time point 2, for all images. The results for each pixel were then plotted as either a positive change >1 mm Hg, a negative change >1 mm Hg, or no change. This analysis was also conducted on the difference images using a threshold of change of 5 mm Hg.

Spatial statistics. To more robustly examine spatial patterns of vascular pO_2, watershed segmentation analysis for spatial change detection was conducted for each experiment. First, the absolute difference between the time-averaged pO_2 for the entire experiment and each individual time point was calculated. The median value of each individual absolute difference image was then subtracted from the image, and watershed segmentation was performed on a pixel by pixel basis using an eight-connected neighborhood. Watershed analysis detects gradients in pO_2 values and segments an image along those gradients; segmented regions can be thought of as pO_2 isobars.

Global Moran's I analysis (33, 34) was performed on all time points for all images to examine if spatial autocorrelations were consistently occurring within an image for disc-shaped spatial ranges with radii of 1, 4, 8, 12, 20, 40, and 100 pixels using a binary weighing function (Supplementary Fig. S1). Global Moran's I analysis was also performed on differences in sequential time images using the same spatial ranges and weighing function as described above.

A two-way ANOVA test was conducted on the resulting Moran's I values to determine if different tumor types had different patterns of spatial autocorrelations. Multiple comparison of the means was done to determine which groups were significantly different using the Bonferroni critical value of $P < 0.05$.

Spatial autocorrelation within a single image was examined using local Moran's I (35). Each time point was checked for local spatial autocorrelations within disc-shaped regions with radii of 1, 4, 8, 12, 20, and 40 pixels using a binary weighing function. Additionally, subsequent time points were subtracted and changes in pO_2 between two time points were examined for local spatial autocorrelations using local Moran's I.

Finally, the averaged map of vascular pO_2 was subjected to discrete Fourier transform to determine the dominant period of fluctuations for each pixel over time. Results from high frequency fluctuations (<5 min) were discarded as the sampling rate of once every 2.5 min could not resolve these high frequencies.

Results

The median vascular pO_2 for all 9L images was 38 (26–40; all values reported are medians and 25–75%) mm Hg, 30 (26–35) mm Hg for FSA, and 22 (19–23) mm Hg for R3230. There was no clear trend over time of increasing or decreasing median pO_2 of the entire image for all the experiments ($P > 0.05$). The representative experiments shown had a median pO_2 of 34 (27–41) for 9L, 21 (16–25) for FSA, and 18 (16–21) mm Hg for R3230 (Fig. 1). These values are higher than previously measured tissue pO_2 values in these same tumor lines (11), consistent with the imaging phosphor largely remaining in the vasculature. Perivascular pO_2 measurements have been made previously in the R3230 tumor using recessed tip oxygen microelectrodes. The data presented here match very well with these microelectrode measurements, which were performed independently (36).

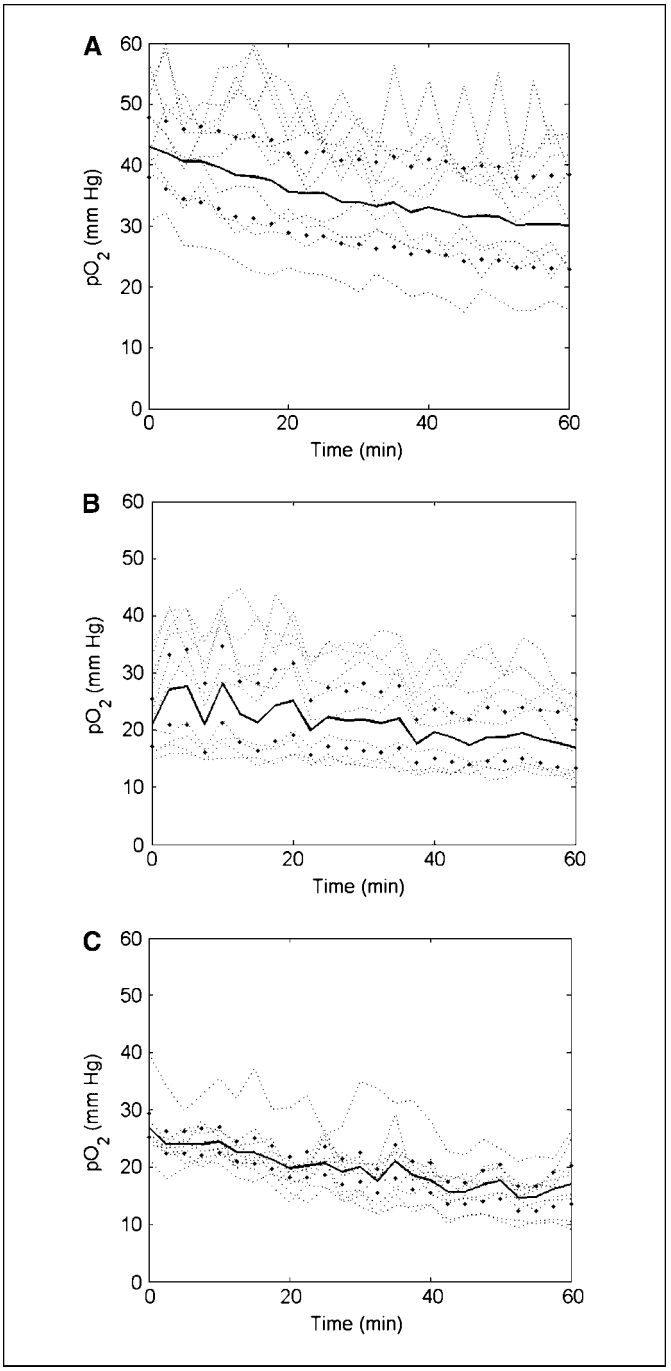

Figure 1. Median pO_2 versus time for 9L (*A*), FSA (*B*), and R3230 (*C*) for representative experiments. Median values of the entire image are plotted as solid lines, and dots show the 25% to 75% range at each time point. For each sample tumor, 10 pixels were randomly selected and pO_2 versus time for each of these pixels was plotted on the same graph as a dashed line.

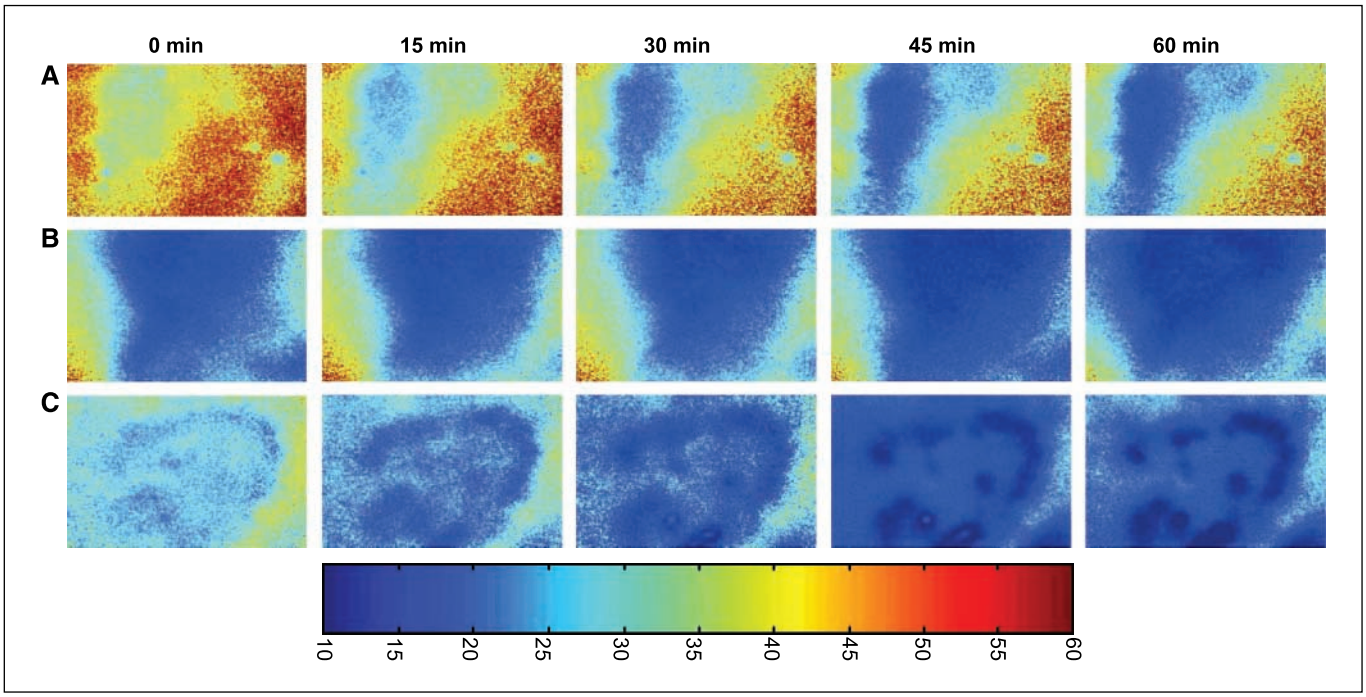

Figure 2. Representative images of PLI data for 9L (*A*), FSA (*B*), and R3230 (*C*). Five time points at 0, 15, 30, 45, and 60 min show pO_2 values for each tumor line.

Although the median pO_2 for a single experiment generally changed only 1 to 2 mm Hg between any 2.5 min measurement interval, plots of randomly selected individual pixel pO_2 versus time reflect significant spatial and temporal variability (Fig. 1) in vascular pO_2. This spatiotemporal variability strongly suggests that sampling a few spatially or temporally discrete pO_2 measurements may not be representative of tumor oxygenation.

O_2 delivery is constantly fluctuating. Examination of the raw PLI images of a representative set of tumors showed different patterns of pO_2 fluctuations for each tumor line (Fig. 2; same representative set of tumors used as samples throughout manuscript; Supplementary Movies S1–S3). 9L images had different areas of the images with their pO_2 fluctuating independently of each other; in the sample shown in Fig. 2, pO_2 on the left side of the image decreases with time, whereas pO_2 on the right side increases. Both FSA and R3230 seemed to have a distinct spatial pattern of pO_2 at the initial time point and pO_2 fluctuations with time maintained these patterns. The FSA sample has an inverted triangular area at lower pO_2 values than the rest of the image. This area initially shrinks and then increases to almost encompass the entire image by the 60-min time point. The R3230 tumor in Fig. 2 has an oval-shaped outline visibly at a lower pO_2 at the first time point, and over time, this oval-shaped outline remains visibly at a lower pO_2.

These observations of differences in vascular pO_2 pattern between tumor types was reinforced through an exploratory analysis looking at the sign of pO_2 changes >1 mm Hg for each pixel from once point to the next (Supplementary Movies S4–S6). Not a single pixel remained unchanged over three sequential time points in all the experiments, and fewer than 5% of the pixels changed <1 mm Hg between any two subsequent time points. These patterns were also visible in the difference images when examining the sign of pO_2 changes >5 mm Hg for each pixel (Supplementary Movies S7–S9). Although there are 2.5-min intervals where only a small percentage of the image shows changes in vascular pO_2 of >5 mm Hg, many of the 2.5-min intervals show 30% to 50% of the image fluctuating at >5 mm Hg.

Tumor type effects spatial distribution of oxygen. Watershed segmentation (Fig. 3) showed distinctly different oxygen isobar patterns for different tumor types. At most time points, 9L was highly segmented, with regions of very different pO_2 values next to each other. R3230 also showed areas which were highly segmented; however, many of the images contained one or two large spatial pO_2 segments. FSA had a great deal of segmentation, but segments with similar pO_2 were almost always conjoined.

Global Moran's *I* analysis showed significant differences in patterns of spatial autocorrelation for the different tumor types (Fig. 4*A*). Generally, spatial autocorrelation decreased as the size of the region examined increased for all tumor types. Both 9L and FSA had several time points, which showed no autocorrelation in *I* values at the smallest spatial range examined (1 pixel radius; Supplementary Table S1) at this spatial range, suggesting that in these images adjoining pixels had pO_2 values which were independent of each other. Within tumor types, *I* values for different spatial ranges tended to be significantly different from each other (Supplementary Table S1). Combined with the knowledge that spatial autocorrelation decreased as the area examined increased, this analysis emphasizes the heterogeneity of O_2 delivery in tumors.

Global Moran's *I* was also used to examine patterns of change in pO_2 between time points (Fig. 4*B*). There was much less spatial autocorrelation in the change in pO_2 values between time points than within a single time point, although all tumor types had some difference images, which showed a high degree of spatial autocorrelation. Spatial autocorrelation further decreased in the difference images as the spatial range examined increased. However, differences in spatial autocorrelation were evident for different tumor types. 9L and R3230 showed significantly less

spatial autocorrelation than FSA at spatial ranges higher than a 1-pixel radius (Supplementary Table S2), and *I* values for these two tumor types were more tightly clustered than FSA at all spatial ranges. FSA and R3230 tend to have significant decreases in Moran's *I* values within each tumor type for small increases in spatial ranges (1 and 4 pixel radii for FSA, 1 and 8 pixel radii for R3230), suggesting changes in pO_2 values over time were spatially coordinated only for small regions in these tumor types.

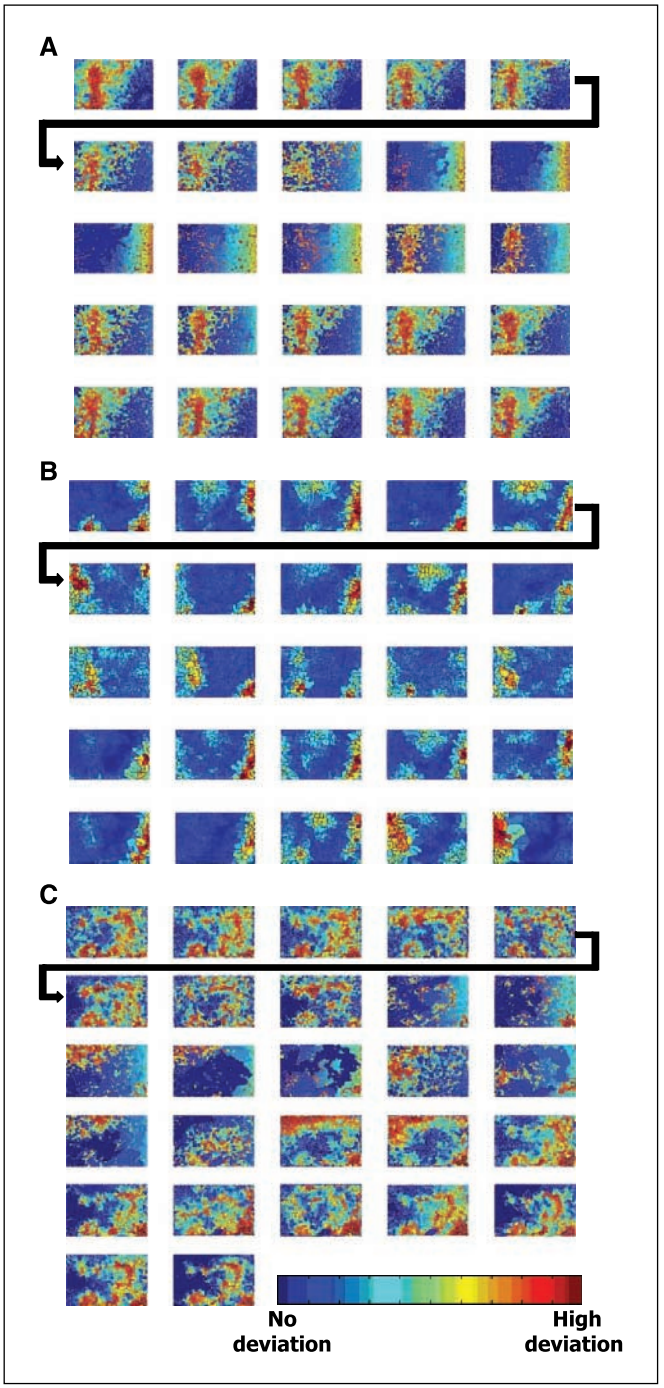

Figure 3. Representative watershed segmentation results for each 2.5-min time point for 9L (*A*), FSA (*B*), and R3230 (*C*). Time increased from left to right, top to bottom, in 2.5-min increments. Watershed segmentation creates boundaries at sharp gradients in pO_2; segmented regions can be thought of as pO_2 isobars. Segments are color-coded by their deviations from the median pO_2 of the image. *Red,* high deviations from the median; *blue,* no deviation from the median.

Global Moran's *I* for an image is an average of normalized local Moran's *I* values for each pixel within that image. Therefore, an examination of local Moran's *I* values for an image offers insight into the areas within an image which have the greatest spatial autocorrelation.

The sample images shown are local Moran's *I* values for a spatial range of an 8-pixel radius (Fig. 5). The 9L tumor had the same general pattern of spatial autocorrelation at all time points, with a large region of spatial autocorrelation on the lower right-hand side. The sample FSA showed an area of high spatial autocorrelation in the inverted triangular region, which increased and decreased in size with time. R3230 showed high spatial autocorrelation at all time points in the oval-shaped outline visible in Fig. 2; this area of high spatial autocorrelation seemed to increase in size with time. Consistent with the global Moran's *I* results for this spatial range, the sample 9L, FSA, and R3230 tumors had a similar proportion of the image showing high spatial coordination.

Figure 6, which shows local Moran's *I* values for difference images for the same sample tumors in Fig. 5, offers insight into the spatial autocorrelation of changes in pO_2 between time points. The 9L sample shows that there is almost no spatial coordination in changes between 2.5 min time points. The sample FSA tumor has noticeably more spatial autocorrelation in pO_2 changes, with regions of high spatial autocorrelation appearing first along the top and lower right side of the image, with a few later time points showing a large region of spatial autocorrelation along the left side. Most time points for the sample R3230 difference images showed a few, highly diffuse spots of high autocorrelation, with most of the image reflecting spatial randomness of pO_2 values. There was a recurring region with high spatial pO_2 autocorrelation in the top left corner of the R3230 sample. The trends in spatial autocorrelation seen in Fig. 6 are consistent with global Moran's *I* values for each tumor type.

For all of the sample tumors shown, the areas of spatial autocorrelation at a single time point are not the same areas which show spatial autocorrelation for pO_2 changes between time points. The distinct pattern of the inverted triangle visible in Fig. 5*B* for FSA is not apparent in Fig. 6*B*; similarly, the oval-shaped outline boldly apparent in Fig. 5*C* for R3230 is almost entirely missing in Fig. 6*C*.

All tumors fluctuate with slow periodicities. Fourier analysis showed the periodicities with the largest pO_2 fluctuation magnitudes were >10 min for all three tumor types. Generally, the three slowest periodicities (ranging from 10 to >40 minutes) for a pixel have a similar order of magnitude contribution to the overall pO_2 fluctuation magnitude; faster fluctuation periodicities have 10^2 to 10^4 lower order of magnitude contribution to the overall pO_2 fluctuation magnitude.

Discussion

The concept of hypoxia being a source for radioresistance goes back to the seminal work of Thomlinson and Gray (37). In this study, the investigators carefully measured the width of the viable rim of biopsies taken from patients with lung tumors and determined that the maximum width tended to be 180 to 200 μm, regardless of the size of the tumor nodule. They concluded that the viable rim width was consistent with the maximum diffusion

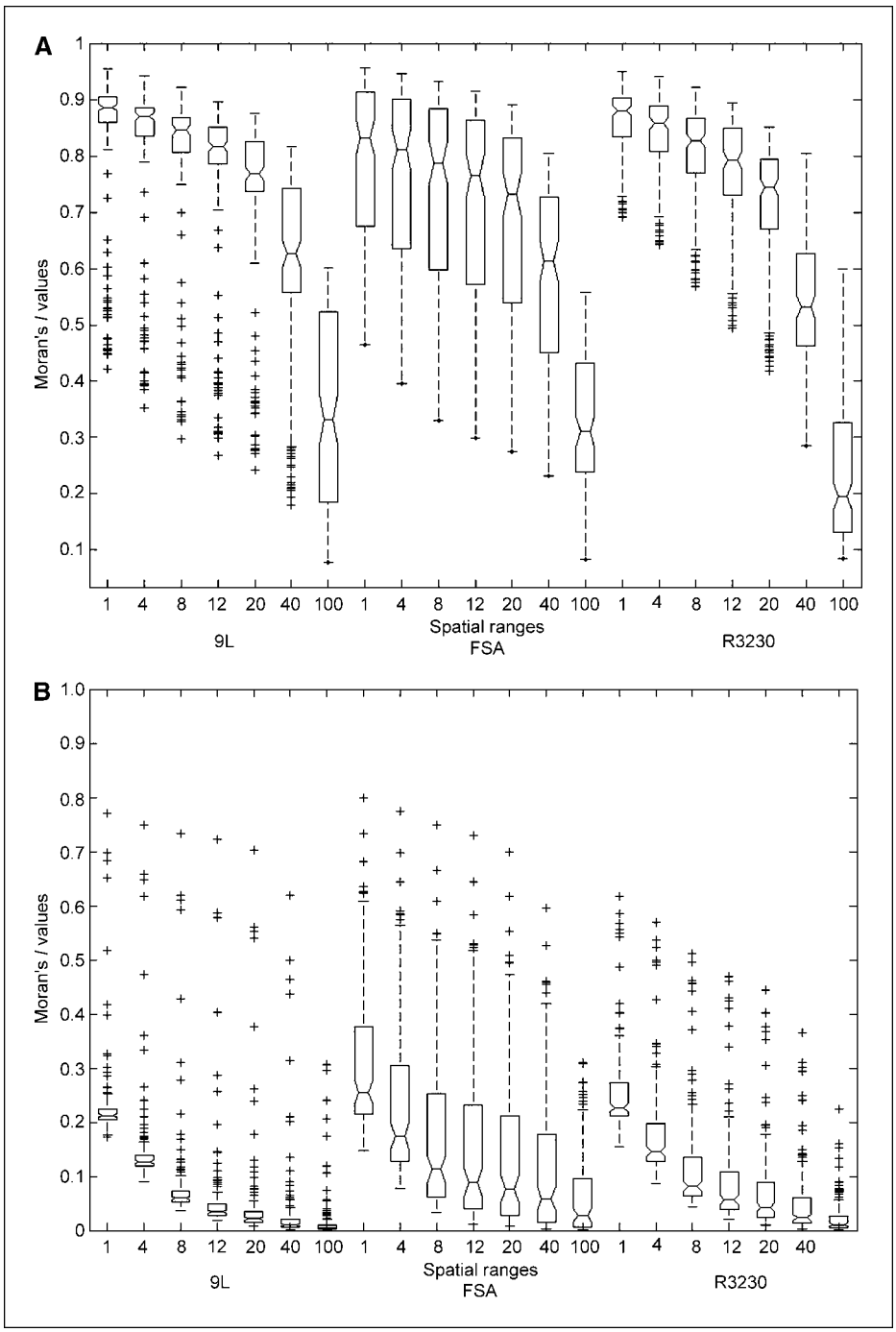

Figure 4. Global Moran's *I* values. *A,* all pO_2 time points for all experiments. *B,* all pO_2 difference images for all time points for all experiments. *Solid lines,* median values; *boxes,* contain 25% and 75%; *error bars,* 1.5× interquartile range; +, *I* values which fall outside 1.5× interquartile range. Moran's *I* values approaching 1 indicate high spatial autocorrelation of pO_2 values, Moran's *I* values of zero indicate spatial randomness. For each tumor type, Moran's *I* is shown for disc-shaped spatial ranges of radii 1, 4, 8, 12, 20, 40, and 100.

distance of oxygen in tumor tissue. Thomlinson and Gray hypothesized that cells that reside near the necrotic edge would be hypoxic and therefore radioresistant. Although this observation spurred a number of clinical trials, it was nearly 30 years before it was definitively shown that hypoxia was a cause for radioresistance in human tumors (38).

Vaupel was among the first investigators to show that human tumors contained hypoxic regions and that the presence of hypoxia was an important prognostic factor in cervix cancer (39). Subsequently, similar reports were published involving a number of human tumors, including head and neck, sarcomas, and prostate cancer (40–42). The work of Thomlinson and Gray alluded to and was based upon the assumption of a steady-state gradient of oxygen from a source vessel, a concept that was further promulgated by the advent of hypoxia marker drugs, which typically exhibit increased binding in tumor cells as a function of their distance from the nearest microvessel. This feature of tumor hypoxia has been termed chronic, implying that cells that located far from a microvessel reside in a constant state of hypoxia.

The notion that tumor cells might be transiently hypoxic as a result of instabilities in tumor blood flow was introduced in the late 1970s in three seminal papers. In one study, Intaglietta and colleagues observed arteriolar vasomotion in feeding vessels of tumors grown in window chambers (43). They reported the

sinusoidal behavior of RBC movement in vessels, presumably caused by this vasomotor activity Yamaura and Matsuzawa irradiated tumors growing in window chambers and carefully monitored the location of tumor regrowth (44). They observed that the tumors almost always regrew at the periphery of the tumors and suggested two potential mechanisms in explanation of this localized radioresistance. In one proposal, cells in the tumor periphery are assumed to be better oxygenated, resulting in a higher growth fraction and a higher fraction of relatively resistant cells in S-phase at the time of irradiation. Yamaura and Matsuzawa also proposed that transient hypoxia could be responsible for radioresistance, as vascular stasis had occasionally been observed at the tumor periphery. Brown showed the reemergence of radiobiologically hypoxic cells 24 hours after administration of a hypoxic cytotoxin, Misonidazole, in the EMT6 tumor (45). This study was the first to show that transient hypoxia could be radiobiologically important.

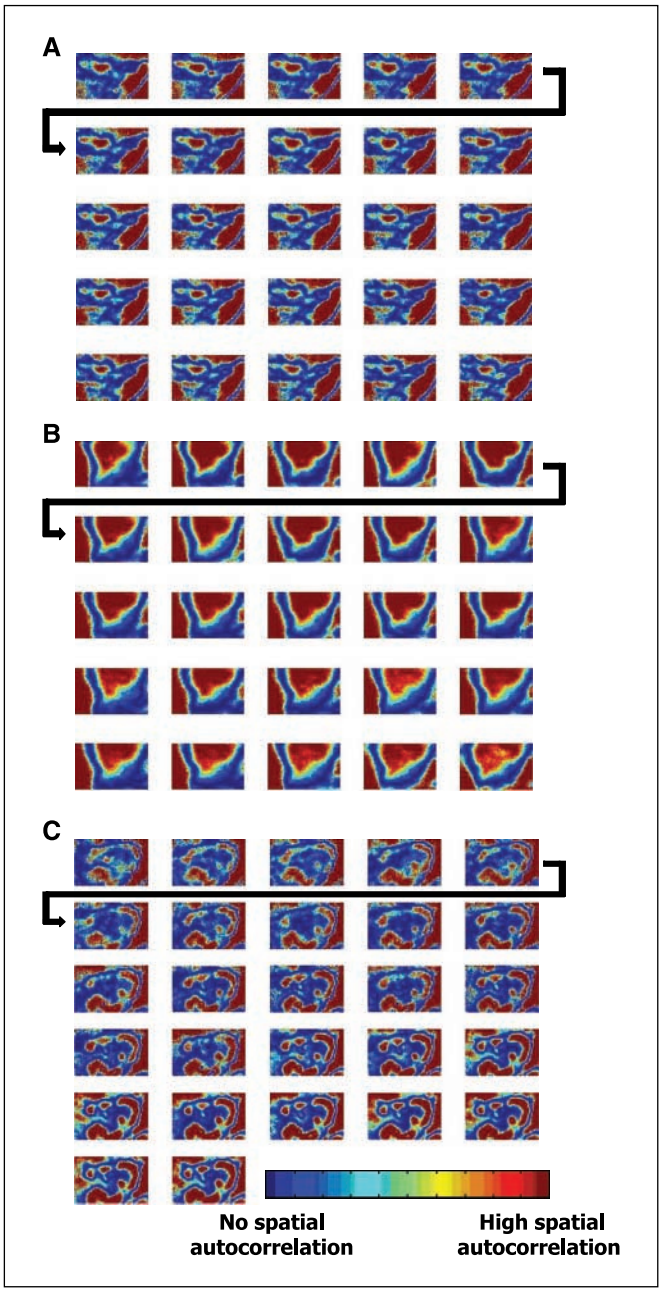

Figure 5. Representative local Moran's *I* results (8-pixel radius spatial range) for each 2.5-min time point for 9L (*A*), FSA (*B*), and R3230 (*C*). Time increased from left to right, top to bottom, in 2.5-min increments. *Red, I* values reflecting high spatial autocorrelation for a pixel; *blue, I* values reflecting no spatial autocorrelation or spatial randomness.

This paper proves our hypothesis that fluctuating vascular oxygenation is a prevalent characteristic of these three tumor lines. The main result of this study is one that has perhaps been intuitively understood but not previously explicitly shown: O_2 delivery to tumor tissue is constantly changing. Previous characterization of hypoxia as perfusion-limited or diffusion-limited are simply the extreme cases of O_2 delivery dominant or O_2 metabolism dominant areas in tumors; most tumor tissue does not distinctly fall into either category and the local pO_2 is heavily influenced by both.

This study shows that up to 50% of tumor vascular pO_2 can change >5 mm Hg within a 2.5-min interval; previous theoretical predictions have calculated that a change in vascular pO_2 of 10 mm Hg can cause a considerable increase ($\sim$30%) in the proportion of severely hypoxic tumor tissue (<3 mm Hg; ref. 46). Although these predictions cannot be directly applied to the data in this study, changes in vascular pO_2 of >5 mm Hg, such as those seen in this study, would certainly be expected to alter the hypoxic fraction of the surrounding tissue. Experimental results have shown that fluctuations in vascular pO_2 result in fluctuations in tissue pO_2 to the maximum oxygen diffusion distance ($\sim$150 μm; ref. 47).

Perhaps the universal characteristic of tumor pO_2 is that the vascular pO_2 fluctuations are occurring at low frequencies or periods on the order of 10s of minutes. This idea is not a new one; the seminal work of Chaplin and colleagues using perfusion markers showed that the injection of dyes 20 minutes apart resulted in marker mismatch in vessels (4). Later studies showed that the significant time scale was at least 15 minutes for perfusion marker mismatch (6), a time scale which has been reinforced with direct measurements of pO_2 fluctuations (5, 9, 11, 12). This study is the first to show that these direct, single-point studies of tumor pO_2 can be generalized to describe the dominant period of pO_2 fluctuations for the entire tumor. A recent publication has shown that pO_2 fluctuations are occurring at dominant periods of 10s of minutes in spontaneous canine tumors (12), suggesting the characteristic behavior of fluctuating pO_2 is not limited to murine tumors or xenografts grown in rodents and may have a common mechanism across all tumors. Studies measuring pO_2 fluctuations in normal tissue (muscle) in rats and mice have not observed significant fluctuations (5, 9).

Although no studies directly measuring fluctuating pO_2 have been done in human tumors, fluctuations in red cell flux have been measured clinically in humans and were shown to occur with a median periodicity of 13 min (range, 4–44 min; ref. 48). Measurements of fluctuating blood flow in different areas within these human tumors also revealed spatial heterogeneity in the fluctuations; spatial heterogeneity in temporal oxygen fluctuations has important implications for optimization of traditional therapies such as radiation. If areas of fluctuating hypoxia were able to be visualized, higher doses of radiation could be delivered to hypoxic areas at a time during which pO_2 values in that area were at the peak of their fluctuations. Further studies examining the spatio-temporal periodicity of tumor oxygenation over a longer timescale (days) relevant to treatment scheduling need to be conducted.

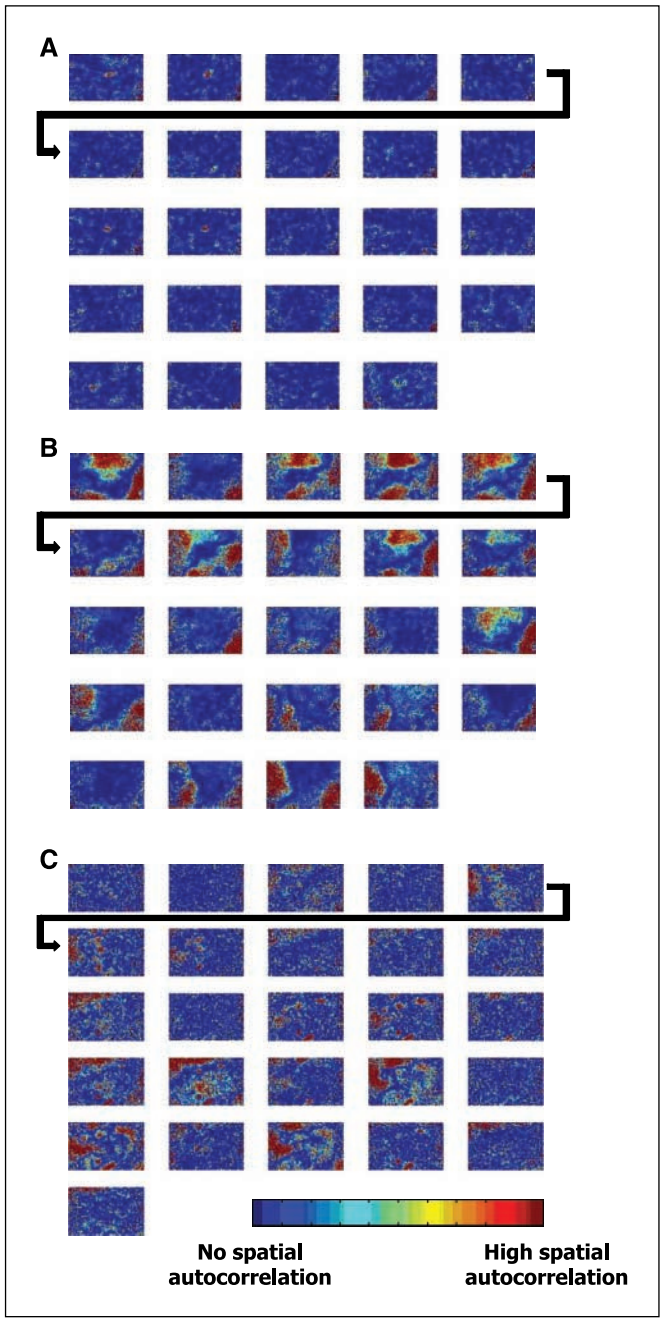

Figure 6. Representative local Moran's I results (8 pixel radius spatial range) for each pO_2 difference image for (*A*) 9L; (*B*) FSA; and (*C*) R3230. Time increased from left to right, top to bottom, in 2.5-min increments. *Red, I* values reflecting high spatial autocorrelation for a pixel; *blue, I* values reflecting no spatial autocorrelation or spatial randomness.

This paper has shown that fluctuations in vascular pO_2 are constantly occurring throughout tumors. Nearly all of the current understanding of tumors and tumor cell adaptation to hypoxia contains the underlying assumption of cellular exposure to chronic hypoxia. However, numerous publications have shown that intermittent hypoxia or hypoxia/reoxygenation events alter the behavior of tumor cells. Graeber and colleagues showed that multiple rounds of hypoxia/reoxygenation selected for apopotosis-resistant tumor cells, with each hypoxic treatment increasing the percentage of p53-deficient cells by 2.4% (20). Another study more broadly showed the potential of intermittent hypoxia to act as a physiologic selective agent for tumor cell mutations: Reynolds and colleagues showed the mutation frequency of tumor cells increased with each cycle of hypoxia exposure (23). Whole-body exposure of tumor-bearing mice to intermittent hypoxia has been shown to result in increased spontaneous metastases in lungs (19) and lymph nodes (18). Recently, a study has shown that fluctuating hypoxia promotes different phenotypes in endothelial and tumor cells than chronic hypoxia, further promoting cells to participate in tumor progression and treatment resistance (21, 49).

The literature also increasingly suggests that the molecular effects of hypoxia will have to be revisited. Studies looking at oxidative stress have shown that cycles of intermittent hypoxia increased HIF-1α protein expression and transactivation function in tumor cells through molecular mechanisms which are distinct from those of chronic hypoxia (25). Activation of *HIF-1* was shown to increase with increasing number of hypoxia/reoxygentation cycles (21, 25). A related study has also shown that intermittent hypoxia also increases c-fos mRNA in tumor and endothelial cells and increased activation of activator protein 1, both of which were abolished through the use of an superoxide dismutase mimetic (24). These studies strongly suggest that intermittent hypoxia is more potent in activating gene expression than chronic hypoxia. Additionally, one study has shown that >200 genes are selectively affected by intermittent, but not chronic, hypoxia (22); this presents a multitude of potential therapeutic targets which are currently overlooked due to a misunderstanding of the prevalence and importance of fluctuating oxygenation in tumors. Given the probable widespread presence of fluctuating hypoxia in human tumors, many more studies need to be done under this new paradigm of tumor physiology.

Spatiotemporal analysis reveals some clues regarding the underlying mechanism(s) of fluctuating hypoxia. Fluctuations in red cell flux, possibly due to vasomotion, are known to cause fluctuations in tumor tissue pO_2 (17, 46, 47). This proposition of fluctuations in red cell flux within tumor vessels is consistent with the analysis shown in Fig. 5: while pO_2 for individual pixels show temporal fluctuations throughout the image, the continuous presence over time of the inverted triangle and oval-shaped outline visible in two of the tumors suggest a network of vessels through which red cells are moving. This result is not unexpected; in prior work with microelectrodes, we found significant fluctuations in tissue pO_2 of regions of 200 to 300 μm in diameter in which small networks of five to six microvessels were involved (47). However, in Fig. 6, autocorrelation of changes in pO_2 between time points is generally not occurring in the locations of the networks in Fig. 5. One potential mechanism for these localized areas of change in pO_2 may be vascular intussusception, which has been shown to locally alter blood flow in experimental tumors with a similar timescale to the one measured in our study (50).

Disclosure of Potential Conflicts of Interest

No potential conflicts of interest were disclosed.

Acknowledgments

Received 11/27/2007; revised 4/29/2008; accepted 5/2/2008.

Grant support: NIH/National Cancer Institute grant CA40355 and Department of Defense grant BC043284.

The costs of publication of this article were defrayed in part by the payment of page charges. This article must therefore be hereby marked *advertisement* in accordance with 18 U.S.C. Section 1734 solely to indicate this fact.

References

1. Hockel M, Schlenger K, Hockel S, Aral B, Schaffer U, Vaupel P. Tumor hypoxia in pelvic recurrences of cervical cancer. Int J Cancer 1998;79:365–9.
2. Vaupel P, Schlenger K, Knoop C, Hockel M. Oxygenation of human tumors: evaluation of tissue oxygen distribution in breast cancers by computerized O_2 tension measurements. Cancer Res 1991;51:3316–22.
3. Rofstad EK, Sundfor K, Lyng H, Trope CG. Hypoxia-induced treatment failure in advanced squamous cell carcinoma of the uterine cervix is primarily due to hypoxia-induced radiation resistance rather than hypoxia-induced metastasis. Br J Cancer 2000;83:354–9.
4. Chaplin DJ, Olive PL, Durand RE. Intermittent blood flow in a murine tumor: radiobiological effects. Cancer Res 1987;47:597–601.
5. Braun RD, Lanzen JL, Dewhirst MW. Fourier analysis of fluctuations of oxygen tension and blood flow in R3230Ac tumors and muscle in rats. Am J Physiol 1999; 277:H551–68.
6. Durand RE, LePard NE. Contribution of transient blood flow to tumour hypoxia in mice. Acta Oncol 1995; 34:317–23.
7. Trotter MJ, Chaplin DJ, Durand RE, Olive PL. The use of fluorescent probes to identify regions of transient perfusion in murine tumors. Int J Radiat Oncol Biol Phys 1989;16:931–4.
8. Baudelet C, Ansiaux R, Jordan BF, Havaux X, Macq B, Gallez B. Physiological noise in murine solid tumours using T2*-weighted gradient-echo imaging: a marker of tumour acute hypoxia? Phys Med Biol 2004;49:3389–411.
9. Brurberg KG, Graff BA, Rofstad EK. Temporal heterogeneity in oxygen tension in human melanoma xenografts. Br J Cancer 2003;89:350–6.
10. Bennewith KL, Raleigh JA, Durand RE. Orally administered pimonidazole to label hypoxic tumor cells. Cancer Res 2002;62:6827–30.
11. Cardenas-Navia LI, Yu D, Braun RD, Brizel DM, Secomb TW, Dewhirst MW. Tumor-dependent kinetics of partial pressure of oxygen fluctuations during air and oxygen breathing. Cancer Res 2004;64:6010–7.
12. Brurberg KG, Skogmo HK, Graff BA, Olsen DR, Rofstad EK. Fluctuations in pO(2) in poorly and well-oxygenated spontaneous canine tumors before and during fractionated radiation therapy. Radiother Oncol 2005;77:220–6.
13. Trotter MJ, Chaplin DJ, Olive PL. Possible mechanisms for intermittent blood flow in the murine SCCVII carcinoma. Int J Radiat Biol 1991;60:139–46.
14. Tufto I, Rofstad EK. Transient perfusion in human melanoma xenografts. Br J Cancer 1995;71:789–93.
15. Trotter MJ, Olive PL, Chaplin DJ. Effect of vascular marker Hoechst 33342 on tumour perfusion and cardiovascular function in the mouse. Br J Cancer 1990;62:903–8.
16. Minchinton AI, Durand RE, Chaplin DJ. Intermittent blood flow in the KHT sarcoma-flow cytometry studies using Hoechst 33342. Br J Cancer 1990;62:195–200.
17. Dewhirst MW, Kimura H, Rehmus SW, et al. Microvascular studies on the origins of perfusion-limited hypoxia. Br J Cancer Suppl 1996;27:S247–51.
18. Cairns RA, Hill RP. Acute hypoxia enhances spontaneous lymph node metastasis in an orthotopical murine model of human cervical carcinoma. Cancer Res 2004; 64:2054–61.
19. Cairns RA, Kalliomaki T, Hill RP. Acute (cyclic) hypoxia enhances spontaneous metastasis of KHT murine tumors. Cancer Res 2001;61:8903–8.
20. Graeber TG, Osmanian C, Jacks T, et al. Hypoxia-mediated selection of cells with diminished apoptotic potential in solid tumours. Nature 1996;379:88–91.
21. Martinive P, Defresne F, Bouzin C, et al. Preconditioning of the tumor vasculature and tumor cells by intermittent hypoxia: implications for anticancer therapies. Cancer Res 2006;66:11736–44.
22. Prabhakar NR. Oxygen sensing during intermittent hypoxia: cellular and molecular mechanisms. J Appl Physiol 2001;90:1986–94.
23. Reynolds TY, Rockwell S, Glazer PM. Genetic instability induced by the tumor microenvironment. Cancer Res 1996;56:5754–7.
24. Yuan G, Adhikary G, McCormick AA, Holcroft JJ, Kumar GK, Prabhakar NR. Role of oxidative stress in intermittent hypoxia-induced immediate early gene activation in rat PC12 cells. J Physiol 2004;557:773–83.
25. Yuan G, Nanduri J, Bhasker CR, Semenza GL, Prabhakar NR. Ca2+/calmodulin kinase-dependent activation of hypoxia inducible factor 1 transcriptional activity in cells subjected to intermittent hypoxia. J Biol Chem 2005;280:4321–8.
26. Papenfuss HD, Gross JF, Intaglietta M, Treese FA. A transparent access chamber for the rat dorsal skin fold. Microvasc Res 1979;18:311–8.
27. Grant JP, Wells SA, Jr. Tumor resistance in rats immunized to fetal tissues. J Surg Res 1974;16:533–40.
28. Wheeler KT, Tel N, Williams ME, Sheppard S, Levin VA, Kabra PM. Factors influencing the survival of rat brain tumor cells after *in vitro* treatment with 1,3-bis(2-chloroethyl)-1-nitrosourea. Cancer Res 1975;35:1464–9.
29. Erickson K, Braun RD, Yu D, et al. Effect of longitudinal oxygen gradients on effectiveness of manipulation of tumor oxygenation. Cancer Res 2003; 63:4705–12.
30. Smith TL, Osborne SW, Hutchins PM. Long-term micro- and macrocirculatory measurements in conscious rats. Microvasc Res 1985;29:360–70.
31. Dewhirst MW, Ong ET, Rosner GL, et al. Arteriolar oxygenation in tumour and subcutaneous arterioles: effects of inspired air oxygen content. Br J Cancer Suppl 1996;27:S241–6.
32. Dunphy I, Vinogradov SA, Wilson DF. Oxyphor R2 and G2: phosphors for measuring oxygen by oxygen-dependent quenching of phosphorescence. Anal Biochem 2002;310:191–8.
33. Cressie N. Statistics for spatial data. New York: Wiley; 1991.
34. Moran PAP. The interpretation of statistical maps. J Am Stat Assoc Ser B 1948;10:243–51.
35. Anselin L. Local indicators of spatial association-LISA. Geograph Anal 1995;27:93–115.
36. Dewhirst MW, Ong ET, Klitzman B, et al. Perivascular oxygen tensions in a transplantable mammary tumor growing in a dorsal flap window chamber. Radiat Res 1992;130:171–82.
37. Thomlinson RH, Gray LH. The histological structure of some human lung cancers and the possible implications for radiotherapy. Br J Cancer 1955;9:539–49.
38. Gatenby RA, Kessler HB, Rosenblum JS, et al. Oxygen distribution in squamous cell carcinoma metastases and its relationship to outcome of radiation therapy. Int J Radiat Oncol Biol Phys 1988;14:831–8.
39. Hockel M, Knoop C, Schlenger K, et al. Intratumoral pO2 predicts survival in advanced cancer of the uterine cervix. Radiother Oncol 1993;26:45–50.
40. Nordsmark M, Bentzen SM, Rudat V, et al. Prognostic value of tumor oxygenation in 397 head and neck tumors after primary radiation therapy. An international multicenter study. Radiother Oncol 2005;77:18–24.
41. Fyles A, Milosevic M, Hedley D, et al. Tumor hypoxia has independent predictor impact only in patients with nodenegative cervix cancer. J Clin Oncol 2002;20:680–7.
42. Movsas B, Chapman JD, Hanlon AL, et al. Hypoxic prostate/muscle pO2 ratio predicts for biochemical failure in patients with prostate cancer: preliminary findings. Urology 2002;60:634–9.
43. Intaglietta M, Myers RR, Gross JF, Reinhold HS. Dynamics of microvascular flow in implanted mouse mammary tumours. Bibl Anat 1977;15:273–6.
44. Yamaura H, Matsuzawa T. Tumor regrowth after irradiation; an experimental approach. Int J Radiat Biol 1979;35:201–19.
45. Brown J. Evidence for acutely hypoxic cells in mouse tumours, and a possible mechanism of reoxygenation. Br J Radiol 1979;52:650–6.
46. Kimura H, Braun RD, Ong ET, et al. Fluctuations in red cell flux in tumor microvessels can lead to transient hypoxia and reoxygenation in tumor parenchyma. Cancer Res 1996;56:5522–8.
47. Lanzen J, Braun RD, Klitzman B, Brizel D, Secomb TW, Dewhirst MW. Direct demonstration of instabilities in oxygen concentrations within the extravascular compartment of an experimental tumor. Cancer Res 2006;66:2219–23.
48. Pigott KH, Hill SA, Chaplin DJ, Saunders MI. Microregional fluctuations in perfusion within human tumours detected using laser Doppler flowmetry. Radiother Oncol 1996;40:45–50.
49. Dewhirst MW. Intermittent hypoxia furthers the rationale for hypoxia-inducible factor-1 targeting. Cancer Res 2007;67:854–5.
50. Patan S, Munn LL, Jain RK. Intussusceptive microvascular growth in a human colon adenocarcinoma xenograft: a novel mechanism of tumor angiogenesis. Microvasc Res 1996;51:260–72.

The Pervasive Presence of Fluctuating Oxygenation in Tumors

Laura I. Cárdenas-Navia, Daniel Mace, Rachel A. Richardson, et al.

Cancer Res 2008;68:5812-5819.